ADVANCED ELECTRONIC MATERIALS Open Access
www.advelectronicmat.de

Degradable and Printed Microstrip Line for Chipless Temperature and Humidity Sensing

James Bourely, Jaemin Kim, Christian Beyer, Oleksandr Vorobyov, Xavier Aeby, Gustav Nyström, and Danick Briand**

Research on chipless and passive architectures for environmental sensing is generating high interest because they do not require any semiconductor components or batteries to operate, thus resulting in an eco-friendlier footprint. This study demonstrates a printed microstrip line with multiple resonators using biodegradable materials to continuously monitor temperature and relative humidity (RH). Constructed with a paper substrate and printed zinc conductive lines, and encapsulated with beeswax to protect against the interference of humidity, the microstrip line integrates spiral-shaped resonators. One resonator operates at 1.2 GHz for temperature sensing, while another, coated with konjac glucomannan serves for relative humidity sensing at 2 GHz. The multi-resonating features allow for a simultaneous assessment of temperature and humidity. The microstrip line displays a linear sensitivity to temperature of −1.35 MHz °C^{-1} and a non-linear relative humidity sensitivity ranging between −0.8 and −8 MHz/%RH from 30% to 70% RH. Its degradation in a lab-made compost for 70 days shows the removal of the transducing layer in 7 days and degradation of the cellulosic substrate starting after 5 weeks. The developed environmental sensing devices are notably promising for future applications in smart packaging and the tracking of goods aiming at the minimization of electronic waste.

1. Introduction

Our reliance on Internet-of-Things electronics is anticipated to double by 2030.[1–3] But, the proliferation of connected devices also results in an escalation in electronic waste.[4] With less than 20% of electronics being properly recycled,[5] novel solutions relying on more eco-friendly materials to simplify recycling and enable circularity, are required.[6]

In recent years, the integration of wireless sensing technologies into logistics operations has revolutionized supply chain management.[7] Wireless sensors have emerged as critical components, enabling real-time monitoring and tracking of goods throughout the supply chain and therefore enhancing efficiency and transparency.[8] With the increasing demand for precise environmental monitoring, the development of wireless devices capable of sensing temperature and relative humidity has received significant attention.[8]

Standard data loggers, integrating temperature and humidity sensing functionalities, are bulky.[9] They typically utilize standard printed circuit board designs made of copper and FR4, powered by a battery and incorporated with a variety of sensors.[10]

Positioned on pellets or within containers during shipment, these loggers are therefore impractical for tracking individual packages in smart packaging applications due to their cost and size.[11]

A promising solution for the cost-effective and scalable deployment of monitoring devices involves leveraging printing techniques and flexible substrates, which hold potential for widespread adoption across various supply chain departments.[12–15] Hybrid-electronic systems, fabricated with printing technologies on flexible substrates and combined with silicon components, have been developed to track environmental parameters for the monitoring of goods.[16–19] They consist of a printed radio frequency (RF) circuit, a sensing unit, an integrated circuit (IC) and energy harvesting components or batteries, all integrated onto a flexible substrate. These various wireless printed sensing platforms were designed to monitor temperature and relative humidity.[20–30] They have the added benefit of allowing interrogation by existing regular Radio Frequency

J. Bourely, J. Kim, D. Briand
Soft Transducers Laboratory (LMTS)
Ecole Polytechnique Fédérale de Lausanne (EPFL)
Rue de la Maladière 71c, Neuchâtel 2000, Switzerland
E-mail: james.bourely@epfl.ch; danick.briand@epfl.ch
C. Beyer, O. Vorobyov
CSEM SA
Rue Jaquet-Droz 1, Neuchâtel 2002, Switzerland
X. Aeby, G. Nyström
Swiss Federal Laboratories for Materials Science and Technology (Empa)
Cellulose & Wood Materials Laboratory
Überlandstrasse 129, Dübendorf 8600, Switzerland
G. Nyström
Department of Health Science and Technology
ETH Zürich
Zürich 8092, Switzerland

The ORCID identification number(s) for the author(s) of this article can be found under https://doi.org/10.1002/aelm.202400229

DOI: 10.1002/aelm.202400229

Identification (RFID) readers. Nevertheless, they still rely on silicon components rendering their end-of-life disposal and recycling complex.[31,32]

Chipless wireless sensors represent a paradigm shift from traditional semiconductor-based integrated circuits.[33–36] These untethered sensors, which do not need active circuitry for data processing and communication, operate on the principle of encoding the information in the frequency and amplitude of electromagnetic (EM) waves.[37,38]

Far-field (distance at which the EM field behave predominantly as a propagating wave) structures are used to maintain a reasonable wireless device size of a few centimetres and to increase operating distance.[39] The far-field tags operate at frequencies in the Ultra-High-Frequency (UHF band = 300 MHz – 3 GHz) and higher. A robust platform for encoding and transmitting information is the microstrip line. This type of chipless device consists of a dielectric substrate layer on which is patterned an electrically conductive trace. It operates based on the modulation of the EM signals along the transmission line. The electric field emanating from the transmission conductor extends beyond the confines of the dielectric material potentially interacting with the surrounding media.[40]

By mechanically deforming, and therefore changing the shape of the conductive layer and the propagating EM wave, strip lines have been applied to monitor the deformation and stress of materials for potential usage as wireless strain gauges for building-health monitoring.[41] Furthermore, the EM modulation of the microstrip line can be made sensitive to environmental parameters such as humidity or temperature, by implementing materials that would have their permittivity or conductance affected by changes in the surrounding environmental conditions.[42] Polyamide, having its dielectric properties sensitive to temperature, was coated on a copper/FR4 microstrip line at 4.5 GHz and used for wireless thermal sensing.[43] By absorbing moisture, various biopolymers like psyllium or alginate deposited on a copper on an FR4 microstrip line at 3.4 GHz were demonstrated to sense relative humidity for applications in contactless RH sensing.[44] Being easily integrated with microfluidics, microstrip line devices measuring the chemical binding of specific analytes on FR4 substrate relying on phenylboronic acid to sense glucose at 1.2 GHz,[45] or using a well to detect the presence lambda DNA up to 17 GHz,[46] have been investigated, showing that microstrip lines could be useful for non-invasive body monitoring or wireless sensing of cell and molecule activity. However, the presented types of microstrip lines still rely on a bulky Vector Network Analyzer to record the signal. Potential real-world applications of microstrip lines for chipless and wireless sensing would involve adding two polarized radiating patch antennas on either side of the microstrip line, increasing the device footprint and would be interrogated using a dedicated reader.[40,47]

By combining the advantages of using printing processes and implementing the chipless principle, different printed chipless RFID tags have been developed for sensing.[48–51] More specifically, wireless printed chipless structures taking the shape of slots or loops have been developed to sense temperature using a thermal-sensitive resistive material affecting the conductivity, frequency and amplitude of the resonator. Examples, such as a PEDOT:PSS layer deposited on a printed silver on PET resonator at 1.2 and 5.8 GHz,[52] carbon applied over a printed silver coil-antenna on PET resonating at 13.58 MHz,[53] or carbon nanotubes over two silver printed split-ring resonators on paper at 2.5 GHz,[54] have been reported. Relative humidity was detected using the interaction between water molecules and moisture-sensitive materials locally changing the permittivity of the resonator. Paper was considered as both active material and substrate with silver-printed ring resonators operating at 300 MHz, 7 GHz and 24 GHz,[55–57] and Nafion was coated over a printed silver ring resonator on paper at 2.8 GHz.[58] Only one known chipless and printed tag combining humidity and temperature sensors has been reported. Its sensing capabilities are achieved with a hygroscopic KaptonHN and thermally sensitive Stanyl polyamide tape positioned along the slot of a silver-printed resonating loop structure made on KaptonHN or PET substrates and resonating between 5 and 25 GHz.[59] These types of low-cost, small footprint and chipless wireless resonators could see application in the field of smart packaging by implementing identification and sensing for the monitoring of perishable goods during transport or storage.[60]

Achieving a high electrical conductivity is essential for ensuring a good RF signal-to-noise ratio and thus providing long-range communication.[33] As a result, most printed wireless devices for environmental sensing have traditionally relied on silver as their primary conductive material, despite employing environmentally friendly substrates such as paper.[11,61] In this context, it is worth noting that, in addition to being an expensive and precious material, silver accounts for 80% of the toxicity of paper-based printed electronics.[62] Alternatively to using silver inks, biodegradable metal particles such as zinc have been demonstrated in wireless applications.[63] An entirely eco-friendly printed chipless sensor combining both temperature and humidity monitoring has yet to be achieved and would be beneficial in enabling sensing while reducing electronic waste.

In this paper, a novel and environmentally non-harmful printed chipless temperature and humidity sensor is proposed. By leveraging additive patterning of eco-resorbable zinc particles, we realize a microstrip line consisting of multi-resonating spiral structures on paper operating between 1 and 3 GHz. The device is encapsulated with beeswax to prevent interfering moisture uptake of the substrate and oxidation of the zinc layer. One resonator is used to sense temperature at 1.2 GHz while being insensitive to humidity. A second resonator at 2.0 GHz is implemented to detect relative humidity with the addition of a super-absorbent plant-based polymer. The multi-resonating design enables the accurate simultaneous assessment of relative humidity and temperature. The microstrip line was shown to decompose in a simulated compost environment over multiple weeks.

By utilizing biodegradable materials and environmentally benign fabrication processes, these eco-friendly chipless devices represent a significant step towards more sustainable sensing systems applied to logistics and beyond.

2. Results and Discussion

2.1. Design and Fabrication of the Microstrip Line

The design of the microstrip line consisting of three spiral-shaped resonators made from biodegradable materials is visible in **Figure 1a**. The microstrip line is made of zinc printed on a

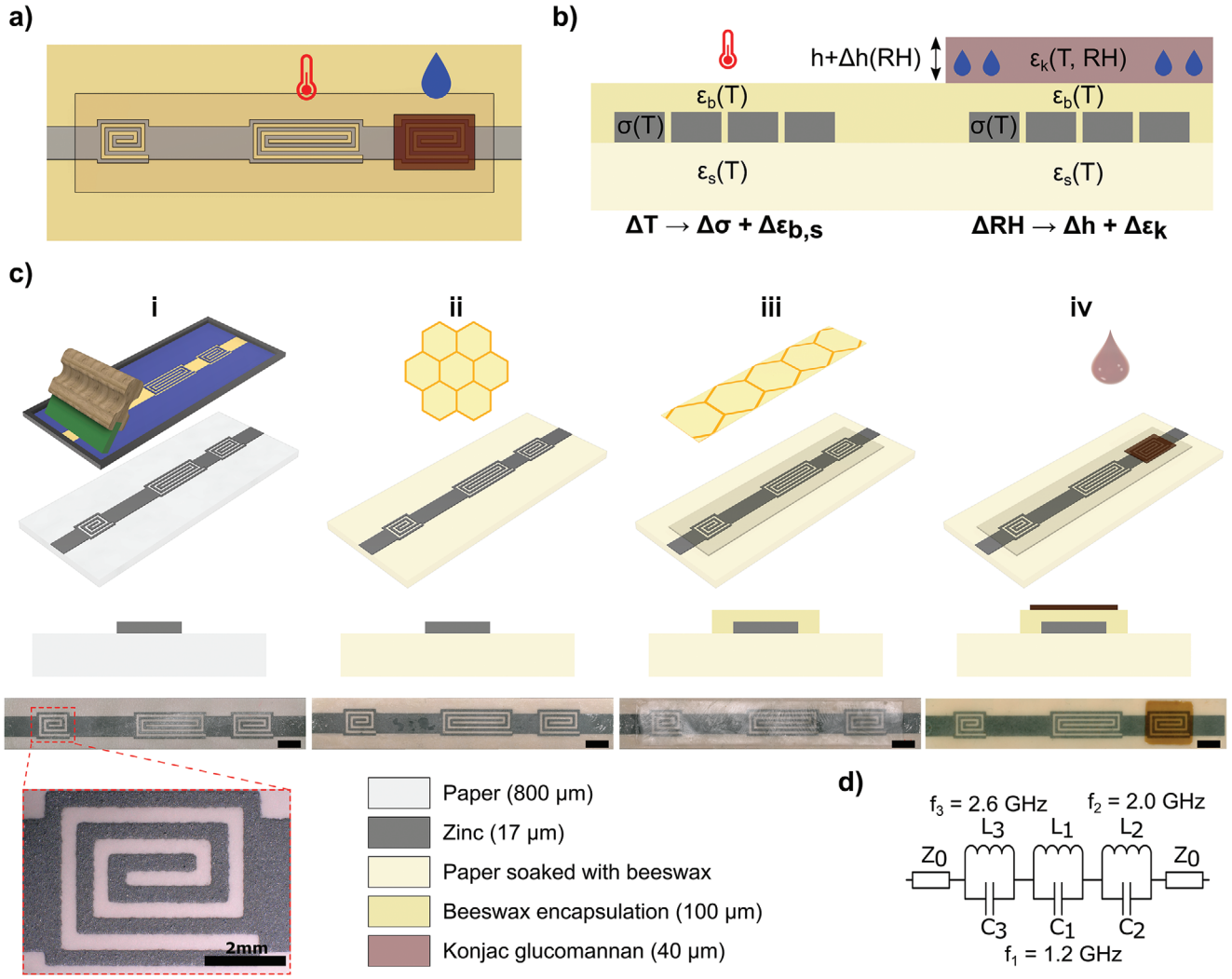

Figure 1. Design of the microstrip line a). Sensing mechanism depicting the effects of temperature and relative humidity on the properties of the materials of the two sensing resonators b). A fabrication process of the eco-friendly microstrip line sensor with corresponding microscope optical images (scale bar = 2 mm) c). Screen printing and hybrid sintering of the zinc (i), beeswax soaking in the paper (ii), beeswax encapsulation lamination over the zinc layer (iii) and konjac glucomannan drop-casting (iv). Equivalent electrical circuit of the transmission line (d).

paper substrate and encapsulated with beeswax and has one resonator coated with konjac glucomannan.

The multiple resonances induced by the spiral resonators can be leveraged for sensing where independent resonators can be designed to target a specific environmental parameter. Two spirals were used for sensing either temperature or relative humidity. The sensing mechanisms for temperature and humidity are depicted in Figure 1b. A temperature change (ΔT) will affect the dielectric permittivities of the beeswax ϵ_b, of the paper substrate soaked with wax ϵ_S and of the konjac ϵ_k, and the conductivity of the zinc σ. Due to the positive thermal coefficient of resistivity of the zinc film,[61] its evolution in resistance will affect the real and imaginary parts of the recorded signal and therefore shift the magnitude of the S_{12} signal.[64] Second, the impedance Z_0 is inversely proportional to the relative permittivity of the dielectric materials.[65] The permittivity of beeswax ϵ_b is, as well, temperature dependant which will locally affect the resonance of the microstrip line.[66] The temperature effect on the permittivity of konjac can be considered as neglectable in comparison to the effect of the absorbed humidity.[67]

A variation in relative humidity (ΔRH) will not affect the hydrophobic beeswax coating, but induce a change of thickness Δh of the super-absorbent konjac glucomannan under the charge or discharge of water (ϵ_{water} = 80), which will result, at the same time, in a modification of its permittivity.[67,68] The combined effects of permittivity and dimension changes of the konjac glucomannan layer due to moisture absorption lead to variations in the RF losses and will be selectively detectable over one of the resonators of the encapsulated microstrip line.

In summary, changes in environmental parameters are influencing the electrical and dielectric properties of the constituting materials along the microstrip line, which result in the alteration of the impedance, capacitance, and RF losses of the different spirals leading to individual shifts of their respective resonance frequency.[64]

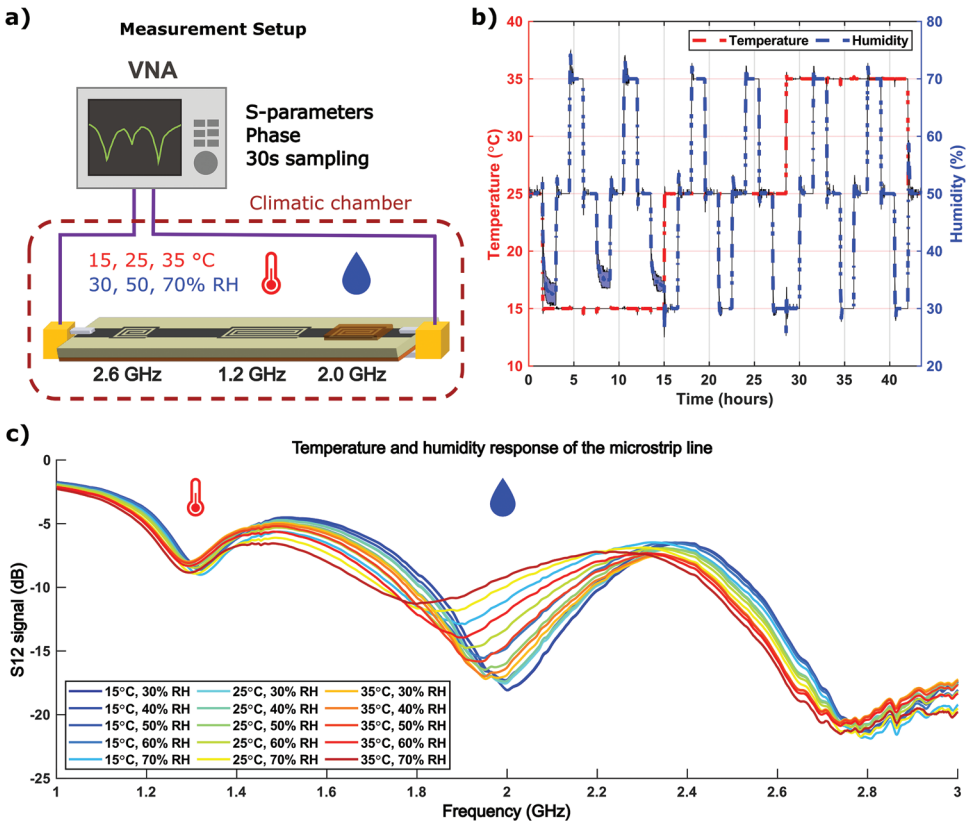

Figure 2. Measurement setup a). Environmental climatic test profile b). Typical recorded data of the S_{12} signal from 1 to 3 GHz for the eco-friendly microstrip line c).

The process flow used to fabricate the microstrip line is available in Figure 1c. Zinc nanoparticles are screen-printed onto an 800 µm-thick paper substrate and sintered following a hybrid sintering process (Figure 1c-i). Applying the optimal process parameters, this method provides the highest electrical conductivity reported for a printed zinc trace of $\sigma = 5.62*10^6\ Sm^{-1}$ or 33% of bulk zinc. With very good reproducibility and high stability over time, this sintering process renders the zinc films suitable for RF applications, as already shown.[63] Because of the porous paper structure, cellulose fibres absorb water, leading to an increase in overall substrate permittivity and loss, thereby causing a shift in the resonance frequency of the resonators, see the effect of humidity on the pristine paper substrate in supplementary Figure S1a (Supporting Information). To mitigate water absorption interference, the paper substrate was saturated with beeswax after printing the zinc layer, serving as a moisture barrier (Figure 1c-ii). To prevent the oxidation of the zinc trace, a 100 µm-thick, 1 cm-wide and 4 cm-long beeswax layer was then laminated over the transmission line. (Figure 1c-iii).[69] Finally, to act as a humidity-sensitive layer, konjac glucomannan, a plant-based super-absorbent capable of gaining fifty times its weight in water, was drop-casted over one of the resonating structures composing the microstrip line (Figure 1c-iv).[70]

Optical imaging of the cross-section of the fabricated device and a confocal microscopy height scan of the zinc layer are depicted in supplementary Figures S2 and S3 (Supporting Information). The thicknesses of the zinc conductor, beeswax encapsulation and konjac glucomannan are measured to be ≈ 17, 100 and 40 µm, respectively.

The microstrip line is designed to operate in the upper limit of the UHF band (1–3 GHz). A simplified equivalent circuit for the three-spiralled microstrip line considered in this work is given in Figure 1d. The spirals were placed at least 5 mm apart to reduce interference with their neighbours. To minimize the total size of the microstrip line, the width of the spirals was kept constant at 4.4 mm with a 400 µm-wide spiral-shaped slot making 3 turns, visible in Figure 1c-i. The obtained resonant frequency f_i for a given spiral is inversely dependent on the capacitance C_i and inductance L_i. Increasing the longitudinal length of the spirals results in a gain in the inductance and capacitance.[71] Thus, a longer spiral will result in a smaller frequency of resonance. The length of each spiral from left to right is 5, 12 and 7 mm, providing resonances at $f_3 = 2.6$ GHz, $f_1 = 1.2$ GHz and $f_2 = 2.0$ GHz, respectively (Figure 1d). The spiral positioned in the middle of the microstrip line resonating at 1.2 GHz is used for temperature sensing and the one on the right, resonating at 2.0 GHz, is applied to humidity sensing. The remaining resonator on the left at 2.6 GHz could be potentially used for differential measurements, act as an identification signature or eventually be functionalized for sensing a specific analyte. The latter, however, could not be exploited in this work due to the high-frequency noise produced by the climatic chamber under operation visible in **Figure 2c**.

A preliminary study, presented in supplementary Figure S4 (Supporting Information), shows that the unexploited

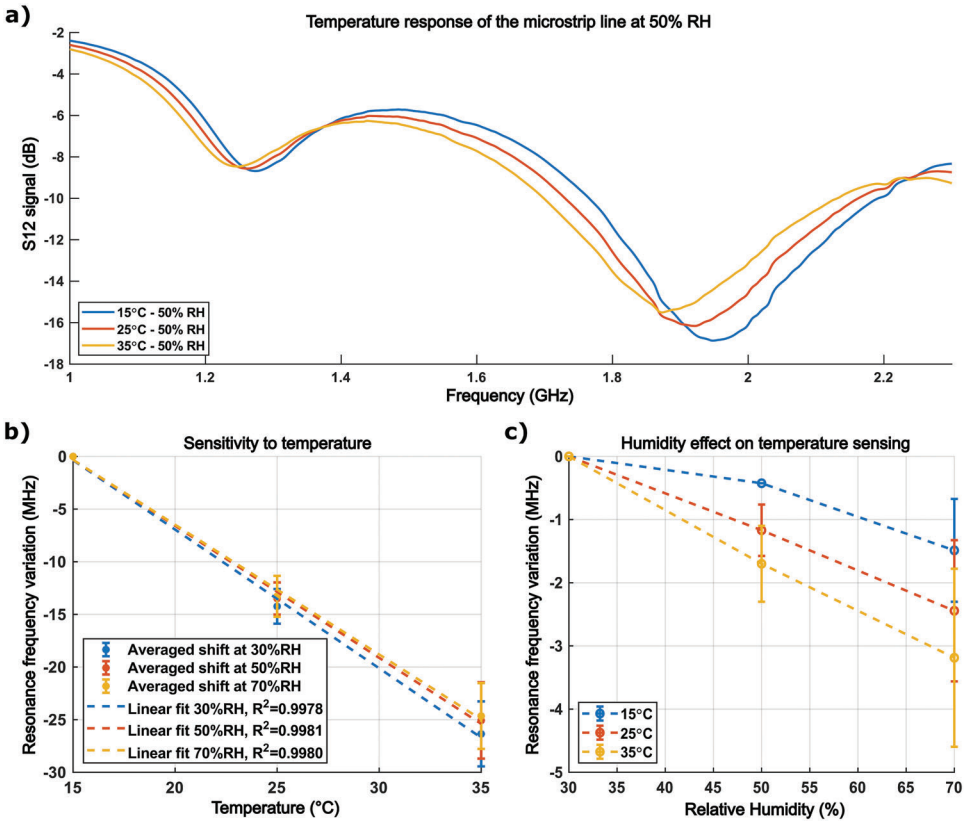

Figure 3. Temperature response and sensitivity. S_{12} signal at 15, 25 and 35 °C of a microstrip line at 50% RH from 1 to 2.3 GHz a). Averaged frequency variation of the first resonating peak at 1.2 GHz in response to temperature at 30%, 50% and 70% RH, with linear approximation (n = 4) b). Resonating frequency position of the first peak against relative humidity at 15, 25 and 35 °C (n = 4) c).

spiral resonating at f_3 could be removed to minimize the device footprint as it has a minimal impact on the frequencies of operation f_1 and f_2 of the two other resonators. Indeed, the variation on the pristine frequencies of resonance f_1 and f_2 induced by removing the last spiral resonating at f_3, is less than 0.2% of the respective resonance frequencies. This variation is even much smaller than the reproducibility deviation of the resonance frequencies f_1 and f_2 between fabrication batches measured to be 7%, as illustrated in Figure S5 (Supporting Information). A way to improve the reproducibility of the fabricated microstrip line would be to utilize an automated screen printer and acid spray dispenser for the sintering of zinc as well as an automated laminator for the deposition of the beeswax encapsulating layer, which would strongly reduce the variabilities associated with the manual fabrication procedures applied in this study.

2.2. Climatic Chamber Testing and Measured Signal

The microstrip line was connected to a Vector Network Analyzer (VNA) to record the complex scatter parameters during climatic testing. The resulting magnitude of the scattering parameter S_{12} and the phase of the device under test (DUT), that is, the microstrip line, were computed.

Figure 2a represents the DUT connected to the VNA and placed inside the climatic chamber. Depicted in Figure 2b is the environmental cycling in temperature and humidity. The microstrip line is analysed at 15, 25 and 35 °C with controlled relative humidity values from 30% to 70% RH. All recorded S_{12} states corresponding to the different combinations of temperature and humidity levels can be seen in Figure 2c. The plotted data is taken at the end of each cycling step to ensure that saturation is reached.

2.3. Temperature Response of the Microstrip Line

The resonance at 1.2 GHz is used to sense temperature variations. For temperature-sensing, we rely on two effects, namely the influence of temperature on both the resistivity of the zinc and the permittivity of the dielectric materials. Those effects are visible in **Figure** 3a where the magnitude and frequency of resonance of the microstrip line are reduced when increasing the temperature. Only the data at 50% RH for the three temperatures was presented for visual clarity but entire recorded signals, showing similar behaviour for other RH percentages, can be seen in Figure 2c.

Analysing the sensitivity of the first resonance at 1.2 GHz versus temperature for 4 different samples shows a very linear behaviour $R^2 > 0.99$ as seen in Figure 3b. From 15 to 35 °C, the total variation in the peak frequency is included between −25 and −26 MHz at all humidity levels tested, resulting in a sensitivity of −1.35 MHz $°C^{-1}$. The insensitivity of this first resonating

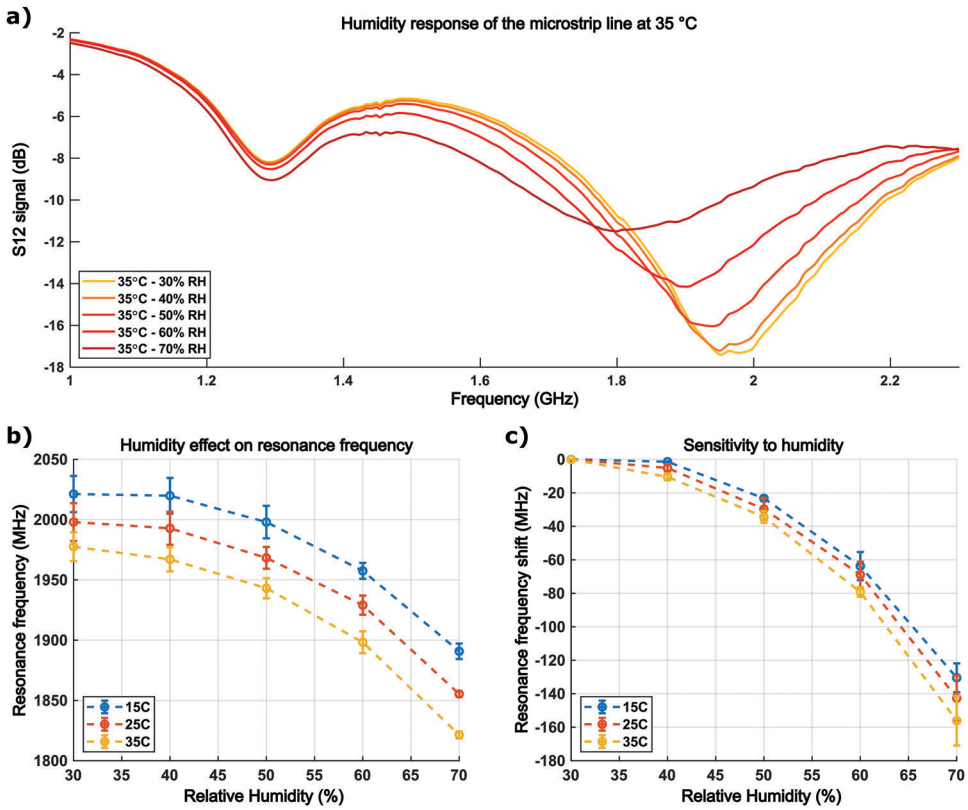

Figure 4. Relative humidity response and sensitivity. S_{12} signal at 30%, 40%, 50%, 60% and 70% RH at a temperature of 35 °C from 1 to 2.3 GHz a). Resonating frequency position of the 2 GHz peak against relative humidity for temperatures of 15, 25 and 35 °C (n = 2) b). Averaged frequency variation of the resonating peak at 2.0 GHz in response to humidity at 15, 25 and 35 °C (n = 2) c).

frequency to moisture, even at a high RH percentage (70%), is provided thanks to the hydrophobic beeswax protection applied. To investigate a temperature range applicable to cold chain monitoring of goods during transport and storage,[72] the microstrip line was also tested from −10 to 35 °C, at ambient humidity due to limitation in the regulation of the RH in the climatic chamber used at these low temperatures. The temperature sensor showed a linearity of $R^2 = 0.989$ for a sensitivity of −1.06 MHz $°C^{-1}$ as seen in Figure S6 (Supporting Information).

In Figure 3c, one can notice that the average resonance frequency changes by 3 MHz across the whole humidity range, which corresponds to a possible maximum error of ≈ 2 °C on the temperature. A possible improvement in the temperature measurement error due to variations in relative humidity might be to increase the thickness of the encapsulating beeswax over the resonator f_1. However, there will be a compromise in thickness to consider since this will induce over the second resonator f_2 a non-desired increase of its sensitivity to temperature while potentially reducing the response to humidity due to excess losses.

This structure entirely made of biodegradable materials achieved a similar temperature sensitivity to what has been reported in the literature, but one needs to keep in mind that those resonators do not have the same shape, and therefore not the same resonance frequency, which influences the sensitivity reached. A wireless copper resonator on ROGER RO4003C substrate showed a variation of −0.1 MHz $°C^{-1}$ at 2.2 GHz,[38] while a printed silver on PVC chipless sensor had a sensitivity of −1.1 MHz $°C^{-1}$ between 1 and 6 GHz.[52] A printed silver on PET resonating tag with polyamide tape at 8.8 GHz showed a change of −0.8 MHz $°C^{-1}$.[59] A summarized comparison of our work with chipless devices used for temperature sensing reported in the literature is available in Table S1 (Supporting Information).

Furthermore, the temperature effect on the phase of the 1.2 GHz resonator as a potential metric for sensing was analysed and is reported in supplementary Figure S7 (Supporting Information). The position of the inversion in the phase corresponding to the resonance is shifted by -1 MHz $°C^{-1}$ and the phase is changed by −0.25 $°°C^{-1}$. Tracking the phase could therefore be an additional method to evaluate temperature variations.

2.4. Relative Humidity Response of the Microstrip Line

The effect of humidity on the S_{12} magnitude of the microstrip line can be seen in **Figure 4**. In Figure 4a, one can view the S_{12} signal as a function of the tested frequency from 1 to 2.3 GHz for different humidity levels at 35 °C (signals for the other temperatures were removed for visual clarity but are available in Figure 2c). Five relative humidity values, from 30% to 70% RH with 10% RH steps, were tested according to a climatic profile available in Figure S6 (Supporting Information). The resonating peak at f_2 = 2.0 GHz in the S_{12} signal shifts to the left with the presence of konjac glucomannan enhancing the losses as it absorbs moisture. Water intake inside the super-absorbent plant-based

biopolymer leads to swelling as seen in supplementary Figure S8 (Supporting Information) where the thickness of konjac nearly doubles when increasing the relative humidity from 30% to 70% RH. The dielectric properties of the konjac glucomannan are modified due to the increase in permittivity and morphology near the resonator. This results in a loss in magnitude supported by a shift in resonance frequency. The humidity-response curves of the microstrip line exhibit a non-linear behaviour noticeable in Figure 4b. This correlates with previous research on the adsorption of water in such biopolymers and with the non-linear swelling behaviour of the konjac aforementioned which results in the permittivity and losses varying in a non-linear manner as well.[68] As the humidity level rises, the polymer matrix can more easily swell which leads to an increase in water intake.[73]

The super-high absorption rate of konjac allows for a full-scale response of −160 MHz from 30% to 70% RH despite the presence of beeswax over the zinc resonator. The sensitivity of the 2.0 GHz resonator to humidity, presented in Figure 4c, is −0.8 MHz/%RH for changes in the lower relative humidity range (below 40% RH) but reaches −8 MHz/%RH between 60% and 70% RH. The standard deviation in humidity-response across n = 2 samples (displayed as error bars in Figure 4b) was computed for all temperatures to be 15 MHz at 30% RH notably due to instabilities in the regulation of the climatic chamber at this low humidity level (visible in Figure 2b), decreasing to 6 MHz at 70% RH. Considering a shift in response of −160 MHz between 30% to 70% RH, this 6 MHz deviation would represent an average error across devices of 3.7% RH and is on par with the RH precision of the climatic chamber (±3% RH). Implementing a fabrication process allowing to reduce the beeswax thickness would diminish the resonator losses and therefore enhance the humidity sensitivity of the device when coated with konjac glucomannan. Nonetheless, the reported relative humidity sensitivity is within the higher range of sensitivities found in the literature thanks to the use of the high absorbent rate of konjac. Chipless inkjet-printed silver resonators on PET operating between 3 and 7 GHz displayed a sensitivity of −6.8 MHz/%RH,[56] a wireless copper resonator on ROGER RO4003C substrate had a variation of −0.5 MHz/%RH at 2.2 GHz,[38] and a wireless silver tag on PET with KaptonHN presented a sensitivity of −2.4 MHz/%RH at 8.5 GHz.[59] A summarized comparison of our work with chipless devices used for relative humidity sensing reported in the literature is available in Table S1 (Supporting Information).

Furthermore, as can be observed in Figure 4c, the reduction in frequency at f_2 of approximately 13 MHz with a rise of 10 °C in temperature at a given relative humidity can be explained by the previously discussed effects of temperature on the resonator. It corresponds to the temperature-sensitivity aforementioned of −1.35 MHz °C^{-1}. A way to reduce the effect of temperature on the resonator f_2 would be to apply, a non-temperature-sensitive and biodegradable interlayer, to be defined, between the konjac and the spiral, knowing that the temperature effects due to the TCR of the zinc would remain. Nevertheless, resonance frequency calibration using the 1.2 GHz resonator could be performed to discriminate the effects of temperature on the 2.0 GHz resonator.

Additionally, as for the previously discussed resonance frequency-variation to moisture, the magnitude evolution of the 2.0 GHz resonator to changes in relative humidity follows, as well, a non-linear trajectory visible in Figure S9a (Supporting Information). In Figure S9b (Supporting Information), the variation of magnitude to humidity is linearly correlated to the variation of the frequency of resonance for said humidity. The monitoring of the magnitude of the S_{12} signal of the 2.0 GHz resonator could also be considered for relative humidity sensing, knowing the temperature from the 1.2 GHz resonator. The change in phase of the 2.0 GHz resonator as a function of the relative humidity is also reported in Figure S10 (Supporting Information). But, the resonance of the phase at 70% RH is no longer properly defined and cannot be detected, limiting the use of the phase for sensing relative humidity.

The continuous response of the 2.0 GHz sensor is depicted in **Figure 5a** for variations in the humidity profile applied in the climatic chamber as shown in Figure S11 (Supporting Information). The climatic chamber has an intrinsic response time measured to be 120 s for every 10% RH step. The S_{12} signal of the DUT is collected every 30 s and the response time of the microstrip line is computed at 63% of the value at saturation, from which is subtracted the response time of the chamber, as well at 63%. Response times of 234, 222 and 216 s are derived for each transition step of 10% RH from 40% to 70% RH at 25 °C. Figure 5b plots the precision of the humidity sensor after two repeated cycles as represented in Figure S11 (Supporting Information). The largest error in precision was measured at 30% and 40% RH with a shift of 5 MHz dropping below the limit of detection of the VNA (LoD = 0.3 MHz) for humidity values above 60% RH, regardless of temperature value. Due to the non-linearity of the humidity response, this 5 MHz difference in the measured frequency would correspond to an error in the relative humidity of 6% below 40% RH and of less than 1% RH above 50% RH. These errors resemble the relative humidity uniformity of the climatic chamber (±3% RH). The reversibility, measured using the climatic cycle in Figure 2b at 35 °C, is plotted in supplementary Figure S12 (Supporting Information) and computed to be 5 MHz at 30% RH, and the highest hysteresis observed in the humidity response was measured to be 5 MHz at 50% amounting to a potential error of 1% RH.

2.5. Stability and Degradation of the Microstrip Line

Finally, the stability of the device at ambient lab conditions and its degradation in lab-made compost were studied.

The evolution of the electrical resistance of the microstrip line with and without beeswax encapsulation, measured over 3 months at ambient temperature and relative humidity, is provided in Figure S1b (Supporting Information). The beeswax encapsulation prevented the oxidation of the biodegradable metal. The drift in resistance of the zinc microstrip line after 12 weeks was reduced from 60% to less than 2% with the implementation of beeswax.

We also assessed the degradation of the paper-based temperature and humidity-sensing microstrip line in a lab-made compost environment over 70 days. As no standards currently exist for the degradation of electronic devices, the compost was designed to respect the ISO standard 20 200 used for the disintegration of polymers in soil. Pictures, presented in **Figure 6**, were taken every week to track the degradation. After 1 week, the konjac

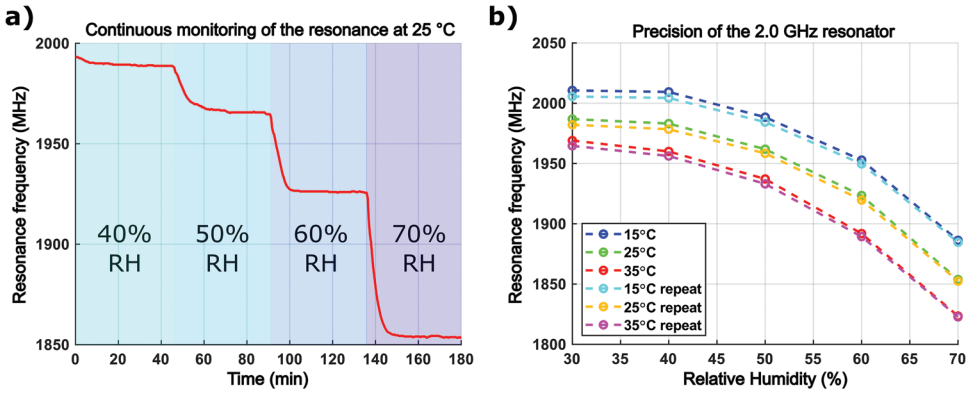

Figure 5. Response of the 2 GHz sensor over one humidity cycle at 25 °C to four 10% RH steps starting at 30% RH up to 70% RH a) and precision of the sensor across two full climatic cycles for 30% RH to 70% RH at 15, 25 and 35 °C b).

completely disappeared and the beeswax was no longer protecting the zinc. This was likely facilitated by the temperature of 58 °C used for the test which is near the melting temperature of the beeswax T_g = 60 °C. On week 2, the zinc, which is no longer encapsulated by the wax deteriorated and after week 5, the paper started to degrade. Finally, on week 10, the paper was decomposed into multiple pieces.

3. Conclusion

In this study, a chipless and degradable multi-resonating microstrip line sensor was printed using zinc on paper and encapsulated with beeswax. The fabricated device is capable of sensing temperatures from −10 to 35 °C and relative humidity from 30% to 70% RH while being fully made of eco-friendly materials. We showed that beeswax, as an encapsulant, can be used to protect the zinc/paper microstrip line from the interference of humidity for reliable temperature sensing with a linear sensitivity between −1.06 and −1.35 MHz °C^{-1}. Konjac glucomannan was applied as a functional layer for humidity-sensing exhibiting a sensitivity of up to −8 MHz/%RH, a maximum hysteresis of 5 MHz, and a response time below 4 min for 10% RH change. The error in reproducibility for the humidity detection across the microstrip lines was 3.7%. The multi-resonating architecture allows for the in-situ compensation of the effect of temperature on the relative humidity sensing response. Higher humidity sensitivities could potentially be reached by decreasing the thickness of the beeswax encapsulation, but would require a specific process development.

While the device remains tethered to a VNA for S_{12} data recording, to have it deployed in the field, future work for a wireless operation would entail the integration of dual-polarized patch antennas on both ends of the microstrip line for signal reception and transmission. To ensure a minimal footprint of the envisioned wireless device while extending its operational range, meticulous design optimization of the antenna patches would be needed.

Being capable of degrading in a compost environment, the developed environmental sensing devices are promising for future applications in the domain of smart packaging, for tracking and monitoring of sensitive goods during their transport and storage, while allowing for the minimization of electronic waste.

4. Experimental Section

Conductive Ink Preparation: Solid zinc spherical nanoparticles (500 nm average diameter, 99.9% purity) were purchased from US Research Nanomaterials. Polyvinylpyrrolidone (PVP) (Mw = 360 K) and pentanol (99%) were purchased from Sigma–Aldrich. Respectively, the three components were mixed in a 25:1:5 weight ratio following the recipe developed by Dr. Fumeaux.[63] PVP and zinc powders were added first to prevent agglomeration with pentanol. The final formulation was homogenized for 30 min at 300 rpm in a planetary mixer (Thinky ARE-250).

Konjac Glucomannan Extract Preparation: Konjac glucomannan flakes were purchased from a local pharmacy. 5 g of konjac flakes were added to 50 mL of deionized water (DIW). The mix was sonicated until the formation of the hydrogel. After 1 h, the konjac hydrogel was placed in 200 mL of IPA for purification and stirred at 300 rpm and 50 °C for 12 h. The

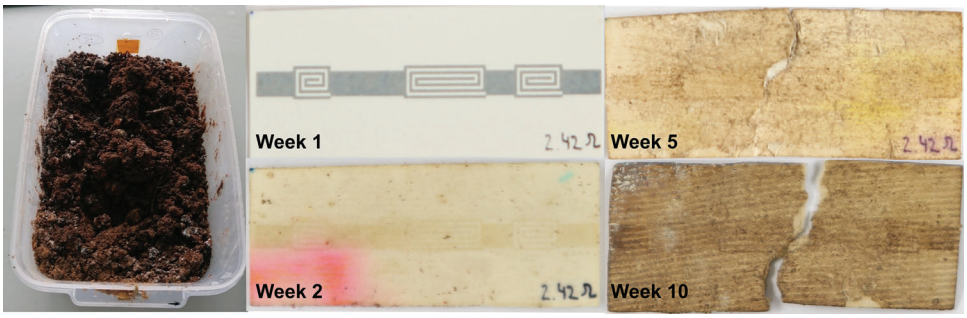

Figure 6. Degradation of the microstrip line in a lab-made compost over 10 weeks.

hydrogel inside the container was removed and the IPA was left to evaporate at 70 °C, leaving a solid residue of konjac. 1 mL of DIW is added and mixed with the remaining solid residue and stored in the fridge at 4 °C for later usage. The konjac glucomannan hydrogel had to be purified with IPA to allow the extract to adhere to the beeswax encapsulation as drop-casting the polymer before purification would lead to delamination.

Device Fabrication: The zinc microstrip line was screen printed onto an ArjoWiggins XD 800 µm-thick paper substrate using a steel-wire mesh purchased from Soral AG, Switzerland. The zinc layer was hybrid sintered using a combination of acetic acid and photonic flash sintering.[63] To ensure the highest electrical conductivity, the optimal sintering parameters were considered. Therefore, 10% acetic acid in DIW was sprayed over the zinc using an airbrush followed by two photonic flashes of 7 J cm^{-2} pulse energy using a Novacentrix PulseForge 1200. 200 mg of beeswax was then melted into the paper at 80 °C during 2 h to ensure the paper was fully saturated, excess beeswax was removed with an absorbent cloth. Saturation of the paper with beeswax was validated visually by observing an optical cross-section as seen in supplementary Figure S13 (Supporting Information). A 100 µm-thick, 1 cm-wide, and 4 cm-long strip of beeswax were formed in a mould and then laminated over the microstrip line to encapsulate the zinc, leaving the extremities of the microstrip line uncovered to allow for electrical connection. Finally, 20 µL of the konjac extract was drop-casted above the 2.0 GHz resonator and confined using a removable 6×8 mm^2 adhesive well.[44] The konjac was left to dry at room temperature overnight and the well was removed to obtain the finalized device.

Data Acquisition during Climatic Testing: Before testing, a copper-tape backplane was added to the prepared biodegradable device. A two-port vector network analyzer (Agilent E5071C) was connected to the microstrip line using a custom magnetic SMA connector (Figure S14, Supporting Information) to prevent soldering on the zinc film. The device under test was placed inside a climatic chamber (Espec SH-262 with ±0.3 °C and ±3% RH uniformity, with %RH control below 15 °C not possible). Temperature and relative humidity in the climatic chamber were recorded every 30 s. Real and imaginary parts of the signal were recorded every 30 s during the climatic cycle and computed for S_{12} magnitude and phase. The computed data was taken at the end of every climatic step by averaging three consecutive recordings. Temperature testing conducted from −10 to 35 °C involved no humidity control with continuous monitoring of the S_{12} signal every 5 s following a temperature ramp.

The detection of the local minimum in the magnitude or phase across the operating frequencies was performed by interpolating, either the S_{12} magnitude or phase, with a 4th-order polynomial function around a given resonating peak (presented in Figure S15, Supporting Information). The polynomial fitting ensures better detection of the S_{12} local minimum at the resonance peak by removing potential noise artifacts. A 4th-order fit was chosen as it interpolates the raw S_{12} signal more precisely compared to a standard RLC circuit matching where R, L and C values need to be fit manually. The 4th-order polynomial fitting error was smaller than the 0.3 MHz limit of detection of the VNA. The various magnitudes and frequencies of resonance were extracted for a total of 4 samples and the results were averaged and presented with standard deviation.

Degradation of the Microstrip Line: The fabricated device was placed into a compost for 70 days and pictures were taken every week to follow the evolution of the degradation. The compost was prepared to recreate 2.2 kg of synthetic solid waste according to Table 1 of ISO 20200 which is used to assess the disintegration of polymers in soil. The sample was placed in a fine-mesh metal bag and buried in the compost with controlled water-content and pH. The reactor was stored at 58 °C in an oven over 10 weeks. After each week, the sample was removed from the bag and a picture was taken. The water and pH were then controlled before placing the sample back into the reactor.

Supporting Information

Supporting Information is available from the Wiley Online Library or from the author.

Acknowledgements

The authors kindly acknowledge funding from the Swiss National Science Foundation and Innosuisse BRIDGE Discovery program for the project "GREENsPACK—Green Smart Packaging" (Grant No.: 40B2-0_187223/1). The authors wish to thank ArjoWiggins Creative Paper now part of the group Fedrigoni Special Papers for providing the paper substrates.

Conflict of Interest

The authors declare no conflict of interest.

Data Availability Statement

The data that support the findings of this study are available from the corresponding author upon reasonable request.

Keywords

chipless microstrip line, eco-friendly sensors, humidity, paper electronics, temperature

Received: March 19, 2024
Revised: June 4, 2024
Published online:

[1] K. Naveed, C. Watanabe, P. Neittaanmäki, *Technol. Soc.* **2018**, *53*, 23.
[2] G. Latif, J. M. Alghazo, R. Maheswar, P. Jayarajan, A. Sampathkumar, in *Integration of WSN and IoT for Smart Cities*, (Eds: S. Rani, R. Maheswar, G. R. Kanagachidambaresan, P. Jayarajan), Springer International Publishing, Cham, **2020**, pp. 103–114.
[3] K. Shafique, B. A. Khawaja, F. Sabir, S. Qazi, M. Mustaqim, *IEEE Access* **2020**, *8*, 23022.
[4] B. Tansel, *Environ. Int.* **2017**, *98*, 35.
[5] V. Forti, C. P. Baldé, R. Kuehr, G. Bel, United Nations University, The Global E-Waste Monitor 2020: Quantities, Flows, and the Circular Economy Potential, Bonn/Geneva/Rotterdam, **2020**.
[6] J. Cui, H. Jørgen Roven, in *Electronic Waste*, Elsevier, Amsterdam, **2011**, pp. 281.
[7] R. Strange, A. Zucchella, *Multinatl. Bus. Rev.* **2017**, *25*, 174.
[8] K. Windt, M. Hülsmann, in *Understanding Autonomous Cooperation and Control in Logistics*, (Eds: M. Hülsmann, K. Windt), Springer Berlin Heidelberg, Berlin, Heidelberg, **2007**, pp. 1–16.
[9] D. F. Kocaoglu, Technology Management in the Energy Smart World (PICMET 2011), IEEE, Piscataway, NJ, **2011**.
[10] C. Connolly, *Sens. Rev.* **2010**, *30*, 192.
[11] J. Zuo, J. Feng, M. G. Gameiro, Y. Tian, J. Liang, Y. Wang, J. Ding, Q. He, *Future Foods* **2022**, *6*, 100198.
[12] H. Landaluce, L. Arjona, A. Perallos, F. Falcone, I. Angulo, F. Muralter, *Sensors* **2020**, *20*, 2495.
[13] V. Subramanian, J. B. Chang, A. De La Fuente Vornbrock, D. C. Huang, L. Jagannathan, F. Liao, B. Mattis, S. Molesa, D. R. Redinger, D. Soltman, S. K. Volkman, Q. Zhang, in *ESSCIRC 2008 –34th Eur. Solid-State Circuits Conf*, IEEE, Edinburgh, UK, **2008**, pp. 17–24.
[14] Y. Bonnassieux, C. J. Brabec, Y. Cao, T. B. Carmichael, M. L. Chabinyc, K.-T. Cheng, G. Cho, A. Chung, C. L. Cobb, A. Distler, H.-J. Egelhaaf, G. Grau, X. Guo, G. Haghiashtiani, T.-C. Huang, M. M. Hussain, B. Iniguez, T.-M. Lee, L. Li, Y. Ma, D. Ma, M. C. McAlpine, T. N. Ng, R. Österbacka, S. N. Patel, J. Peng, H. Peng, J. Rivnay, L. Shao, D. Steingart, et al., *Flex. Print. Electron.* **2021**, *6*, 023001.

[15] X. Aeby, J. Bourely, A. Poulin, G. Siqueira, G. Nyström, D. Briand, *Adv. Mater. Technol.* **2022**, *8*, 2201302.
[16] A. Ilic, T. Staake, E. Fleisch, *IEEE Pervasive Comput.* **2009**, *8*, 22.
[17] Y. Khan, A. Thielens, S. Muin, J. Ting, C. Baumbauer, A. C. Arias, *Adv. Mater.* **2020**, *32*, 1905279.
[18] B. B. Maskey, J. Lee, Y. Majima, J. Kim, J. Lee, G. Bahk, G. R. Koirala, G. Cho, J. Sun, K. Shrestha, S. Kim, M. Park, Y. Kim, H. Park, S. Lee, Y. Han, *IEEE Sens. J.* **2020**, *20*, 2106.
[19] A. Vena, B. Sorli, Y. Belaizi, B. Saggin, J. Podlecki, in 2018 2nd URSI Atl. Radio Sci. Meet. -RASC, IEEE, Meloneras, **2018**, pp. 1.
[20] C. L. Baumbauer, M. G. Anderson, J. Ting, A. Sreekumar, J. M. Rabaey, A. C. Arias, A. Thielens, *Sci. Rep.* **2020**, *10*, 16543.
[21] J. Fernandez Salmeron, F. Molina-Lopez, A. Rivadeneyra, A. Vasquez Quintero, L. F. Capitan-Vallvey, N. F. De Rooij, J. Banqueri Ozaez, D. Briand, A. J. Palma, *IEEE Sens. J.* **2014**, *14*, 4361.
[22] E. Smits, J. Schram, M. Nagelkerke, R. Kusters, G. Van Heck, V. Van Acht, M. Koetse, J. Van Den Brand, G. Gerlinck, in Proc. IMCS 2012, AMA Service GmbH, Von-Münchhausen-Str, Wunstorf, Germany, Nürnberg/Nuremberg, Germany, **2012**, *49*, pp. 403–406.
[23] A. V. Quintero, F. Molina-Lopez, E. C. P. Smits, E. Danesh, J. van den Brand, K. Persaud, A. Oprea, N. Barsan, U. Weimar, N. F. de Rooij, D. Briand, *Flex. Print. Electron.* **2016**, *1*, 025003.
[24] E. Abad, S. Zampolli, S. Marco, A. Scorzoni, B. Mazzolai, A. Juarros, D. Gomez, I. Elmi, G. Cardinali, J. Gomez, *Sens. Actuators, B* **2007**, *127*, 2.
[25] Y.-F. Wang, T. Sekine, Y. Takeda, K. Yokosawa, H. Matsui, D. Kumaki, T. Shiba, T. Nishikawa, S. Tokito, *Sci. Rep.* **2020**, *10*, 2467.
[26] P. Escobedo, M. M. Erenas, N. López-Ruiz, M. A. Carvajal, S. Gonzalez-Chocano, I. De Orbe-Payá, L. F. Capitán-Valley, A. J. Palma, A. Martínez-Olmos, *Anal. Chem.* **2017**, *89*, 1697.
[27] A. Beniwal, P. Ganguly, A. K. Aliyana, G. Khandelwal, R. Dahiya, *Sens. Actuators, B* **2023**, *374*, 132731.
[28] C. Mousoulis, X. Jiang, N. Raghunathan, D. Peroulis, in 2017 IEEE Sens, IEEE, Glasgow, **2017**, pp. 1.
[29] D. Barmpakos, G. Kaltsas, *Sensors* **2021**, *21*, 739.
[30] J. Gao, J. Siden, H.-E. Nilsson, M. Gulliksson, *IEEE Sens. J.* **2013**, *13*, 1824.
[31] P. Jiang, M. Harney, Y. Song, B. Chen, Q. Chen, T. Chen, G. Lazarus, L. H. Dubois, M. B. Korzenski, *Procedia Environ. Sci.* **2012**, *16*, 485.
[32] European Commission, Directorate General for Environment, Umweltbundesamt GmbH, Study on Quality Standards for the Treatment of Waste Electrical and Electronic Equipment (WEEE): Final Report, Publications Office, Luxembourg, **2021**.
[33] S. Preradovic, N. C. Karmakar, *Multiresonator-Based Chipless RFID: Barcode of the Future*, Springer, New York, **2012**.
[34] N. C. Karmakar, E. M. Amin, J. K. Saha, *Chipless RFID Sensors*, Wiley, Hoboken, New Jersey, **2016**.
[35] V. Sharma, M. Hashmi, *IEEE Access* **2021**, *9*, 79264.
[36] A. Ahmadihaji, R. Izquierdo, A. Shih, *IEEE Sens. J.* **2023**, *23*, 11356.
[37] K. Finkenzeller, D. Müller, K. Finkenzeller, K. Finkenzeller, *RFID Handbook: Fundamentals and Applications in Contactless Smart Cards, Radio Frequency Identification and near-Field Communication*, Wiley, Chichester, **2010**.
[38] F. Requena, N. Barbot, D. Kaddour, E. Perret, in 2021 IEEE MTT- Int. Microw. Symp. IMS, IEEE, Atlanta, GA, USA, **2021**, pp. 545–548.
[39] K. V. S. Rao, P. V. Nikitin, S. F. Lam, *IEEE Trans. Antennas Propag.* **2005**, *53*, 3870.
[40] Y. J. Zhang, R. X. Gao, Y. He, M. S. Tong, *IEEE Trans. Antennas Propag.* **2019**, *67*, 1428.
[41] M. Herbko, P. Lopato, *Sensors* **2019**, *19*, 3989.
[42] R. Garg, I. Bahl, M. Bozzi, *Microstrip Lines and Slotlines*, Artech House, London, UK, **2013**.
[43] W. M. Abdulkawi, A.-F. A. Sheta, *Sens. Actuators Phys.* **2020**, *309*, 112025.
[44] J. Bourely, L. De Sousa, N. Fumeaux, O. Vorobyov, C. Beyer, D. Briand, *Micro Nano Eng* **2023**, *19*, 100185.
[45] G. R. Koirala, E. S. Kim, N.-Y. Kim, *IEEE Access* **2018**, *6*, 60968.
[46] M. Godfrey, D. Ewert, R. Striker, B. Braaten, *Sensors* **2023**, *23*, 5193.
[47] A. Bansal, R. Gupta, *Int. J. Inf. Technol.* **2020**, *12*, 149.
[48] S. K. Behera, N. C. Karmakar, *IEEE Microw. Mag.* **2021**, *22*, 64.
[49] P. Herrojo, M. Mata-Contreras, *Sensors* **2019**, *19*, 3385.
[50] M. Gee, C. Anandarajah, *Sensors* **2019**, *19*, 4829.
[51] F. Bibi, C. Guillaume, N. Gontard, B. Sorli, *Trends Food Sci. Technol.* **2017**, *62*, 91.
[52] M. Bhattacharjee, F. Nikbakhtnasrabadi, R. Dahiya, *IEEE Internet Things J* **2021**, *8*, 5101.
[53] A. Albrecht, J. F. Salmeron, M. Becherer, P. Lugli, A. Rivadeneyra, *IEEE Sens. J.* **2019**, *19*, 12011.
[54] A. Vena, L. Sydänheimo, M. M. Tentzeris, L. Ukkonen, in 2013 Eur. Microw. Conf., Nuremberg, Germany, October, **2013**, pp. 9-12.
[55] Y. Feng, L. Xie, Q. Chen, L.-R. Zheng, *IEEE Sens. J.* **2015**, *15*, 3201.
[56] M. Borgese, F. A. Dicandia, F. Costa, S. Genovesi, G. Manara, *IEEE Sens. J.* **2017**, *17*, 4699.
[57] W. Islam, A. Habib, M. Y. Umair, Z. Zahid, *Arab. J. Sci. Eng.* **2023**, *48*, 14697.
[58] G. Marchi, E. Zanazzi, V. Mulloni, M. Donelli, L. Lorenzelli, *IEEE J. Flex. Electron.* **2023**, *2*, 145.
[59] M. Nadeem, A. Habib, M. Y. Umair, *Heliyon* **2024**, *10*, e26494.
[60] P. Fathi, N. C. Karmakar, M. Bhattacharya, S. Bhattacharya, *IEEE Sens. J.* **2020**, *20*, 9618.
[61] H. Rahmani, D. Shetty, M. Wagih, Y. Ghasempour, V. Palazzi, N. B. Carvalho, R. Correia, A. Costanzo, D. Vital, F. Alimenti, J. Kettle, D. Masotti, P. Mezzanotte, L. Roselli, J. Grosinger, *IEEE J. Microw.* **2023**, *3*, 237.
[62] J. H. F. Conceição, M. Party, D. Curtil, L. Švecová, N. Marlin, N. Reverdy-Bruas, *Flex. Print. Electron.* **2023**, *8*, 035014.
[63] N. Fumeaux, D. Briand, *npj Flexible Electron.* **2023**, *7*, 14.
[64] J. C. Rautio, V. Demir, *IEEE Trans. Microwave Theory Tech.* **2003**, *51*, 915.
[65] D. M. Pozar, *Microwave Filter*, Wiley, New York, **2020**.
[66] S. P. Chakyar, T. A. Shanto, A. Murali, S. K. Sikha, N. Paul, J. Andrews, V. P. Joseph, in 2016 IEEE MTT- Int. Microw. RF Conf. IMaRC, IEEE, New Delhi, **2016**, pp. 1–4.
[67] K. Kohyama, K. Y. Kim, N. Shibuya, K. Nishinari, A. Tsutsumi, *Carbohydr. Polym.* **1992**, *17*, 59.
[68] X. J. Fan, S. W. R. Lee, Q. Han, *Microelectron. Reliab.* **2009**, *49*, 861.
[69] N. Fumeaux, M. Kossairi, J. Bourely, D. Briand, *Micro Nano Eng.* **2023**, *20*, 100218.
[70] J. Wu, X. Deng, X. Lin, *Radiat. Phys. Chem.* **2013**, *83*, 90.
[71] Z. Li, S. Bhadra, *Sens. Actuators, A* **2019**, *299*, 111581.
[72] H. M. Stellingwerf, A. Kanellopoulos, J. G. van der Vorst, J. M. Bloemhof, *Transp. Res. Part Transp. Environ.* **2018**, *58*, 80.
[73] S. Geng, R. Lin, M. Chen, S. Liu, Y. Wang, *Front. Chem. Eng. China* **2009**, *3*, 357.